Generalized Brillouin diagrams for evanescent waves in metamaterials with interelement coupling

E. Tatartschuk,[1] A. Radkovskaya,[2] E. Shamonina,[1,*] and L. Solymar[3]

[1]*Erlangen Graduate School in Advanced Optical Technologies, University of Erlangen-Nuremberg, Paul-Gordan Str. 6, D-91052 Erlangen, Germany*

[2]*Magnetism Division, Faculty of Physics, M. V. Lomonosov Moscow State University, Leninskie Gory, Moscow 119992, Russia*

[3]*Optical and Semiconductor Devices Group, Electrical and Electronic Engineering (EEE) Department, Imperial College, Exhibition Road, London SW7 2BT, United Kingdom*

(Received 6 October 2009; revised manuscript received 3 January 2010; published 5 March 2010)

A graphical representation for two-dimensional periodic structures is introduced that provides the full information contained in the dispersion equation: not only for the pass band but for the neighboring stop bands as well. It is a seamless natural extension of Brillouin diagrams obtained by adding eight new zones which incorporate the properties of evanescent waves. The accuracy of the infinite lattice approximation is tested both by simulations and experiments using magnetoinductive waves. For waves propagating in one direction and evanescent in the other direction, the results of the three different methods are shown to be in good agreement. The versatility of the new representation and its applicability to the design of near-field manipulating metamaterials is discussed.

DOI: 10.1103/PhysRevB.81.115110 PACS number(s): 41.20.Jb, 42.25.Bs, 42.70.Qs, 73.20.Mf

I. INTRODUCTION

Waves in periodic structures have been studied for over a century. Lippmann[1] made color photographs in 1894 by creating periodic variation in the dielectric constant in an emulsion. Diffraction of x rays in solids started in the 1910s (see, e.g., Ref. 2). The basic relationship in all these cases is between **k**, the three-dimensional wave vector, and ω, the frequency of the wave. In the two-dimensional (2D) case the most popular representation is by diagrams, named after Brillouin,[3] in which constant ω curves are displayed in the k_x, k_y plane. Most of the information is contained in the first Brillouin zone but occasionally as, e.g., in Umklapp[4] processes, higher zones may also have to be taken into account. This representation was conceived for illustrating in a clear and graphic manner the essential properties of propagating waves. Evanescent waves have received much less attention although the neglect can hardly be justified on theoretical grounds. They are of course absent when the medium can be regarded as homogeneous and of infinite dimension but whenever the medium considered happens to be finite (usually, it is) evanescent waves play a role. The best known examples are surface waves and the phenomenon of total internal reflection. For periodic structures with definite pass bands and stop bands the study of evanescent waves is of the utmost importance. The very existence of photonic crystals depends on finding frequency bands in which there are only evanescent waves in all possible directions (see, e.g., Ref. 5). For facilitating the calculation of interface effects in photonic crystals Hsue and Yang[6] and Hsue *et al.*[7] introduced an extended plane-wave expansion which included evanescent waves. In the latter paper they plotted constant frequency curves for the first and higher Brillouin zones which are the result of both propagating and evanescent modes. A quite different generalization of Brillouin diagrams is due to Baccarelli *et al.*[8] It was introduced for periodic structures of finite transverse dimensions to show leakage effects which incorporate not only the various radiation regimes but also leakage into surface waves supported by a dielectric substrate.

A new impetus to the study of evanescent waves was given by Pendry's[9] proposal of the "perfect" lens achievable by negative index media.[10–12] The perfection depends there on the excitation of surface waves on both boundaries of a slab. For a more general study of surface waves that includes the effect of negative permittivity and permeability see, e.g., Ref. 13.

It is often assumed, by lecturers and students alike, that for a 2D periodic structure the isofrequency curves in the k_x, k_y plane give the full information about the lossless dispersion equation. This is incorrect in practically every case of interest. Specifying the frequency and a real value of (say) k_x and determining the value of k_y from the dispersion equation we may find that it is imaginary, or complex with a real part equal to π. None of the present methods of graphical representation can account for this in a single diagram. Our aim in the present paper is to generalize the concept of Brillouin zones by including evanescent waves. We can do so by adding eight new zones to the first Brillouin zone. We shall be able to ask the questions: which waves propagate and which waves are evanescent, what is the rate of decay, and how the decay occurs, monotonically or with alternating phase?

For showing the properties of evanescent waves we need a testing ground. The ideal candidates are magnetoinductive (MI) waves. They owe their existence to magnetic coupling between elements, small relative to the free space wavelength. They were introduced by Shamonina *et al.*[14,15] in 2002 not long after the advent of the new subject of metamaterials. Experimentally, slow waves of coupling between metamaterial elements have been proven to exist in metamaterials in the entire frequency range from MHz (Refs. 16 and 17) over GHz (Ref. 18) to hundreds of THz.[19–21] For any particular realization MI waves can propagate in a limited

band but that band may be anywhere in a region from RF frequencies to infrared and possibly beyond. Alu and Engheta[22] recently proposed a "magnetic molecule" with a resonant frequency in the visible. Liu *et al.*[23] analyzed a one-dimensional (1D) structure of subwavelength elements with submicron dimensions. Their simulations showed that waves could propagate on such structure due to coupling (both magnetic and electric) between the elements. However, we need not be concerned with the various frequency regions because the basic physical principles are essentially independent both of the resonant frequency and of the size of the elements. In the present study our generalized Brillouin diagrams will be related to ω_0, the resonant frequency of the element, and plotted in terms of the relative frequency ω/ω_0.

There is now a large literature on various aspects of MI waves, in particular on propagating waves, dispersion, forward waves, backward waves, spatial resonances, retardation, excitation, positive and negative refraction, reflection, diffraction and defects, waveguide components, biperiodic structures, imaging, waves in a ring structure, and parametric amplification (see, e.g., Refs. 24 and 25). Interaction of magnetoinductive and electromagnetic waves leads to strong spatial dispersion of the effective-medium parameters,[26,27] an effect unaccounted for in a simplified effective-medium model which neglects interaction between elements. Note that magnetoinductive waves also appear under the names of magnetization waves[19] and magnetic plasmons,[20,21] and, when the coupling between the elements is electric, the logical term is electroinductive waves.[23,28] We wish to emphasize that while MI waves are our favorite candidates for showing the relationships between evanescent and propagating waves, the technique is directly applicable to discrete resonant arrays (e.g., nanoparticle arrays[29]) and, with some modifications, to that large family of waves on periodic systems (e.g., phonon polaritons) which have solutions involving both propagating and evanescent waves.

In Sec. II we shall derive the 2D dispersion equation of MI waves with the aid of the Lagrangian for magnetically coupled resonant circuits. In Sec. III we present the generalized Kirchhoff equations (GKE), a very general relationship indeed. We shall refer to the calculations based on GKE as simulations. The reason is that, like numerical packages, it is a blunt instrument. One inserts the calculated or measured mutual impedances and the details of the excitation, and out comes the current distribution. The technique is analytical in the sense that there is an analytical expression into which the parameters need to be inserted but it offers no physical intuition so our practice is to use it in combination with more intuitive techniques.

In Sec. IV we come to the main message of this paper, the generalization of the Brillouin diagrams by including evanescent waves. We provide a classification of the generalized Brillouin diagrams for metamaterial structures with isotropic and anisotropic coupling coefficients. In Sec. V we briefly review the eigenfunctions of the current in order to facilitate the comparisons between the dispersion equation and GKE solutions which is performed in Sec. VI for a set of 29×29 elements. The magnetoinductive near-field lens[30,31] is reinterpreted in Sec. VII in terms of generalized 2D theory, and experimental results confirming the theory are shown. Conclusions are drawn in Sec. VIII.

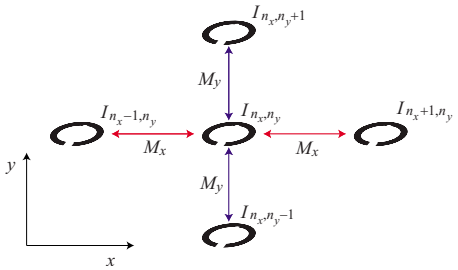

FIG. 1. (Color online) Schematic representation of the near-field coupling between nearest neighbors in a 2D metamaterial.

II. 2D DISPERSION EQUATION OF MAGNETOINDUCTIVE WAVES FOR A RECTANGULAR LATTICE

The metamaterial elements are assumed in the form of capacitively loaded loops which might be the actual realization[16] or may just represent resonant elements like split ring resonators. In a 2D rectangular geometry the element located at n_x,n_y is shown in Fig. 1 together with its nearest neighbors. Figure 2 shows two examples of 2D rectangular arrangements, planar-planar and planar-axial configurations. The elements are coupled to each other by the magnetic fields generated. The dispersion equation for this case has already been derived with the aid of Kirchhoff's voltage equations in one of the first papers[15] written on the properties of MI waves. We shall show here briefly an alternative derivation based on a Lagrangian as introduced for the 1D case by Liu *et al.*[20]

Assuming only nearest-neighbor coupling the Lagrangian for an infinite assembly of identical elements in the nearest-neighbor approximation may be written in the form

$$\mathcal{L} = \frac{1}{2}\sum_{n_x,n_y}\left\{L\dot{q}^2_{n_x,n_y} - \frac{1}{C}q^2_{n_x,n_y} + M_x\dot{q}_{n_x,n_y}(\dot{q}_{n_x-1,n_y} + \dot{q}_{n_x+1,n_y}) + M_y\dot{q}_{n_x,n_y}(\dot{q}_{n_x,n_y-1} + \dot{q}_{n_x,n_y+1})\right\}, \quad (1)$$

where L and C are the inductance and capacitance of the element, M_x and M_y are the mutual inductances in the x and y directions respectively, q_{n_x,n_y} is the charge on the capacitor in element n_x,n_y, and the dot denotes time derivative. Equation (1) may be converted into a differential equation with the aid of the Euler equation (see, e.g., Ref. 20)

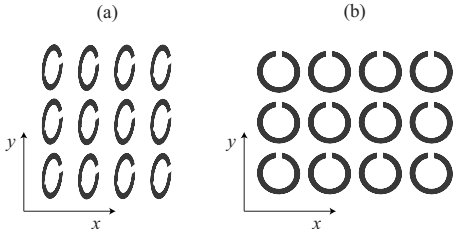

FIG. 2. Examples of metamaterials supporting magnetoinductive waves in the (a) planar-axial and (b) planar-planar configuration.

$$\frac{d}{dt}\left(\frac{\partial \mathcal{L}}{\partial \dot{q}_{n_x,n_y}}\right) - \frac{\partial \mathcal{L}}{\partial q_{n_x,n_y}} = 0. \tag{2}$$

Performing the operations and considering that the current I is the differential of the charge we find the differential equation

$$L\frac{dI_{n_x,n_y}}{dt} + \frac{1}{C}\int I_{n_x,n_y}dt + M_x\left(\frac{dI_{n_x-1,n_y}}{dt} + \frac{dI_{n_x+1,n_y}}{dt}\right) + M_y\left(\frac{dI_{n_x,n_y-1}}{dt} + \frac{dI_{n_x,n_y+1}}{dt}\right) = 0. \tag{3}$$

It needs to be noted that by using the Lagrangian we have adopted here the physicists' starting point. Electrical engineers start immediately with Eq. (3) which is the well-known Kirchhoff equation.

Since we are not interested in the electric and magnetic field distributions we shall assume the solution in the form of plane waves as follows:

$$I_{n_x,n_y} = I_0 e^{i[(k_x d_x n_x + k_y d_y n_y) - \omega t]}, \tag{4}$$

where I_0 is a constant, ω is the angular frequency, k_x and k_y are the wave numbers, and d_x and d_y are the separation of the elements in the x and y directions, respectively.

In order to simplify the notations we shall introduce the normalized variables

$$\zeta_x = k_x d_x \quad \text{and} \quad \zeta_y = k_y d_y, \tag{5}$$

where $\zeta_x = \zeta_x' + i\zeta_x''$ and $\zeta_y = \zeta_y' + i\zeta_y''$, complex values being allowed. The dispersion equation is then obtained in the form

$$1 - \frac{\omega_0^2}{\omega^2} + \kappa_x \cos\zeta_x + \kappa_y \cos\zeta_y = 0, \tag{6}$$

where $\kappa_x = 2M_x/L$, $\kappa_y = 2M_y/L$, and $\omega_0 = 1/\sqrt{LC}$. For a range of frequencies within the pass band,

$$(1 + |\kappa_x| + |\kappa_y|)^{-1/2} \le \frac{\omega}{\omega_0} \le (1 - |\kappa_x| - |\kappa_y|)^{-1/2}, \tag{7}$$

both ζ_x and ζ_y can be real; i.e., there are propagating solutions in both directions. However, Eq. (6) allows at any frequency for the existence of waves evanescent in one or in both directions. Note that with our choice of currents [Eq. (4)] for the waves to decline ζ_x'' and ζ_y'' must be positive.

Note that in the simple 1D case the bands for evanescent and propagating waves do not overlap. The band of the propagating waves is located around the resonant frequency, the band of monotonically decaying evanescent waves is below the pass band for positive coupling coefficient, and the band of decaying evanescent waves with currents in neighboring elements being in antiphase is above the pass band. The two types of bands of evanescent waves interchange in case of negative coupling coefficient. In the 2D case however propagating and evanescent waves may coexist at the same frequency, a feature which may be employed for the realization of near-field lenses. In the literature, the "classical" 2D Brillouin diagrams relate k_x, k_y and the frequency to each other. There is no information about evanescent waves. This is clearly incomplete. We shall propose a representation which will in a seamless manner add that information to the "classical" diagrams.

III. GENERALIZED KIRCHHOFF EQUATION (GKE)

This is a simple but powerful numerical method which we have employed before (see, e.g., Refs. 15 and 32) in order to find the current distribution in the elements for a given excitation. If we apply a voltage to element n then the generalized Kirchhoff law gives

$$V_n = \sum_{n,m} Z_{n,m} I_m, \tag{8}$$

where I_m is the current in element m, $Z_{n,n} = Z_0$ is the self-impedance and $Z_{n,m}$ is the mutual impedance between elements n and m $(n \neq m)$. If there are N elements Eq. (8) may be written in the matrix form as

$$\mathbf{V} = Z\mathbf{I}, \tag{9}$$

where

$$\mathbf{V} = \begin{pmatrix} V_1 \\ V_2 \\ \vdots \\ V_N \end{pmatrix}, \quad \mathbf{I} = \begin{pmatrix} I_1 \\ I_2 \\ \vdots \\ I_N \end{pmatrix}, \tag{10}$$

and Z is the impedance matrix. Note that this formulation is much more general than the 2D dispersion equation discussed in the previous section. First it includes excitation and second we do not need to specify in advance whether we are talking about a one, two or three-dimensional lattice. In fact, there is no need to have a periodic structure either (for an example where the positions of the elements can be arbitrary, see Ref. 33). All that matters is that we know the mutual impedances between any two elements. The current distribution may then be found by inverting the impedance matrix. Note that in the 1D case when only nearest-neighbor interactions are considered Z is a tridiagonal matrix.

IV. GENERALIZATION OF BRILLOUIN DIAGRAMS

The first Brillouin zone for a square lattice extends from $0 < \zeta_x < \pi$ in the x direction and $0 < \zeta_y < \pi$ in the y direction. If we want to add information about the evanescent waves we must realize that there are two kinds of evanescent waves in a lossless medium. One that declines monotonically as a function of distance, and the other one that declines while changing its phase from element to element by π. Calling the monotonically declining wave an e^{m}-wave, the alternately declining one, an e^{a}-wave, and the propagating one a p-wave, the following combinations may exist considering both the x and y directions

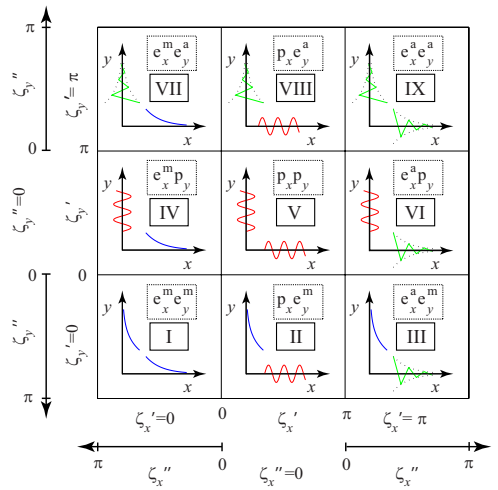

FIG. 3. (Color online) Schematic representation of the generalized Brillouin diagram including zones I–IX with combinations of propagating (p), evanescent monotonic (e^{m}) and evanescent alternating (e^{a}) waves in the x and y directions.

$$e_x^{\mathrm{m}}e_y^{\mathrm{a}}, \quad p_x e_y^{\mathrm{a}}, \quad e_x^{\mathrm{a}}e_y^{\mathrm{a}},$$

$$e_x^{\mathrm{m}}p_y, \quad p_x p_y, \quad e_x^{\mathrm{a}}p_y,$$

$$e_x^{\mathrm{m}}e_y^{\mathrm{m}}, \quad p_x e_y^{\mathrm{m}}, \quad e_x^{\mathrm{a}}e_y^{\mathrm{m}}, \tag{11}$$

amounting to nine zones altogether. This is shown schematically in Fig. 3. There is one familiar zone, and eight new zones which need to be explained. The familiar zone, $p_x p_y$, may be seen in Fig. 3 as zone number V in which waves propagate in both directions. Consequently, ζ_x' and ζ_y' vary from 0 to π.

Next to zone V is zone IV ($e_x^{\mathrm{m}}p_y$). At the boundary of zones V and IV we find that $\zeta_x=0$ and ζ_y' varies from 0 to π. However, in zone IV ζ_x'' now represents a monotonically declining wave, attenuation increasing as ζ_x'' increases from 0 to π in the negative x direction. Note that the choice of π for the left-hand edge of the box is arbitrary. Higher attenuation would, of course, also be possible but we shall not be concerned with those cases.

Zone VI ($e_x^{\mathrm{a}}p_y$) is to the right of zone V. On the boundary of the two zones $\zeta_x'=\pi$ and ζ_y' varies between 0 and π. Now the wave propagates in the y direction and declines alternately in the x direction. Alternate decline means that ζ_x' remains equal to π and ζ_x'' increases from 0 to π.

Zone II ($p_x e_y^{\mathrm{m}}$) is below zone V. Along the common boundary ζ_x' increases from 0 to π. There is monotonic decline in the y direction; the rate of decline increases as ζ_y'' increases from 0 to π.

Zone VIII ($p_x e_y^{\mathrm{a}}$) is above zone V. Along the common boundary ζ_x' increases from 0 to π. There is alternate decline in the y direction: $\zeta_y'=\pi$ and ζ_y'' increases from 0 to π.

Now remain zones I ($e_x^{\mathrm{m}}e_y^{\mathrm{m}}$), III ($e_x^{\mathrm{a}}e_y^{\mathrm{m}}$), VII ($e_x^{\mathrm{m}}e_y^{\mathrm{a}}$), and IX ($e_x^{\mathrm{a}}e_y^{\mathrm{a}}$) in which the waves decline in both directions. In zone I both declines are monotonic: $\zeta_x'=\zeta_y'=0$, and ζ_x'' and ζ_y'' increase from 0 to π. In zone IX both declines are alternate: ζ_x' and ζ_y' are equal to π and ζ_x'' and ζ_y'' increase from 0 to π. In zone III the decline in the x direction is alternate whereas it is monotonic in the y direction. $\zeta_x'=\pi$, $\zeta_y'=0$ and both ζ_x'' and ζ_y'' increase from 0 to π. Finally in zone VII the decline in the x direction is monotonic and alternate in the y direction: $\zeta_x'=0$, $\zeta_y'=\pi$, ζ_x'' and ζ_y'' both increase from 0 to π.

Note that the ω/ω_0=constant contour lines in zones II, IV, VI, and VIII allow one to determine simultaneously the value of the propagation constant in one direction and of the evanescent decay in the perpendicular direction, while zones I, III, VII, and IX contain contour lines of decay rate in both directions. It needs to be emphasized again that the complex values of both ζ_x and ζ_y are continuous across all zone boundaries. This is a necessary condition for the ω/ω_0=constant curves to be also continuous in the plane of this new representation.

The ranges of frequencies for the nine zones depend critically on the values of the coupling coefficients. In principle they can be quite high. For the axial configuration the limiting value is 2 whereas in the planar configuration it tends toward minus unity. Under practical conditions they are usually much smaller. We shall provide below the ranges of the constant frequency curves in each zone under the assumption that $|\kappa_x|,|\kappa_y|<0.5$.

For positive κ_x and negative κ_y [planar-axial arrangement of Fig. 2(a)] the ranges of frequencies are given by

$$\mathrm{I,IX}: \forall \quad \omega,$$

$$\mathrm{II}: \omega \geq \omega_0(1+\kappa_x+\kappa_y)^{-1/2},$$

$$\mathrm{III}: \omega \geq \omega_0(1-\kappa_x+\kappa_y)^{-1/2},$$

$$\mathrm{IV}: \omega \leq \omega_0(1+\kappa_x+\kappa_y)^{-1/2},$$

$$\mathrm{VI}: \omega \geq \omega_0(1-\kappa_x-\kappa_y)^{-1/2},$$

$$\mathrm{VII}: \omega \leq \omega_0(1+\kappa_x-\kappa_y)^{-1/2},$$

$$\mathrm{VIII}: \omega \leq \omega_0(1-\kappa_x-\kappa_y)^{-1/2}, \tag{12}$$

while for both κ_x and κ_y negative [planar-planar arrangement in Fig. 2(b)] they are given by

$$\mathrm{I}: \omega \geq \omega_0(1+\kappa_x+\kappa_y)^{-1/2},$$

$$\mathrm{II}: \omega \geq \omega_0(1-\kappa_x+\kappa_y)^{-1/2},$$

$$\mathrm{III,VII}: \forall \quad \omega,$$

$$\mathrm{IV}: \omega \geq \omega_0(1+\kappa_x-\kappa_y)^{-1/2},$$

$$\mathrm{VI}: \omega \leq \omega_0(1-\kappa_x+\kappa_y)^{-1/2},$$

$$\mathrm{VIII}: \omega \leq \omega_0(1+\kappa_x-\kappa_y)^{-1/2},$$

$$\mathrm{IX}: \omega \leq \omega_0(1-\kappa_x-\kappa_y)^{-1/2}, \tag{13}$$

and zone V is still determined by Eq. (7). These conditions simplify, in the antisymmetric planar-axial case with $\kappa_x=-\kappa_y=|\kappa|$, to

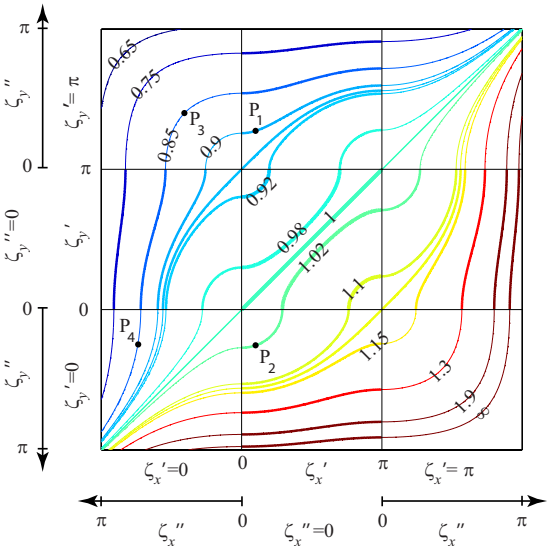

FIG. 4. (Color online) Dispersion curves in the new representation for an antisymmetric planar-axial structure with $\kappa_x=0.1$ and $\kappa_y=-0.1$. Points P_1 to P_4 are discussed in the text.

$$\text{I,IX:}\ \forall\quad \omega,$$

$$\text{II,VI:}\omega \geq \omega_0,$$

$$\text{III:}\omega \geq \omega_0(1-2|\kappa|)^{-1/2},$$

$$\text{IV,VIII:}\omega \leq \omega_0,$$

$$\text{VII:}\omega \leq \omega_0(1+2|\kappa|)^{-1/2}, \tag{14}$$

and, in the symmetric planar-planar case with $\kappa_x=\kappa_y=-|\kappa|$, to

$$\text{I:}\omega \geq \omega_0(1-2|\kappa|)^{-1/2},$$

$$\text{II,IV:}\omega \geq \omega_0,$$

$$\text{III,VII:}\ \forall\quad \omega,$$

$$\text{VI,VIII:}\omega \leq \omega_0,$$

$$\text{IX:}\omega \leq \omega_0(1+2|\kappa|)^{-1/2}. \tag{15}$$

As a first example let us take

$$\kappa_x = 0.1, \quad \kappa_y = -0.1, \tag{16}$$

an antisymmetric planar-axial configuration of split rings. The three parameters, ω/ω_0, κ_x and κ_y, define completely the dispersion equation. It is plotted in the new representation in Fig. 4 for $\omega/\omega_0=0.65,\ldots,\infty$. It may be seen immediately that in zone V, in which both waves propagate, the waves have a forward character in the x direction (corresponding to the positive coupling coefficient) and a backward character in the y direction ($\kappa_y<0$). Equation (14) provides the ranges of frequencies for zones I–IX. Note that all curves traverse several zones, starting in zone I and ending in zone IX.

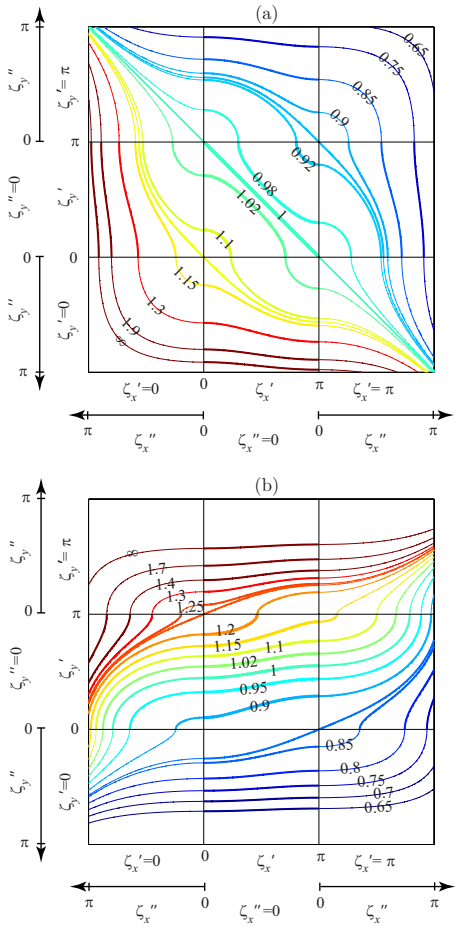

FIG. 5. (Color online) Dispersion curves for a symmetric planar-planar structure, $\kappa_x=\kappa_y=-0.1$ (a) and for an asymmetric planar-axial structure, $\kappa_x=-0.05$ and $\kappa_y=0.3$.

In Fig. 5(a) we plot the dispersion curves for the symmetric planar-planar configuration in which both coupling coefficients are negative and equal. They are taken as $\kappa_x=\kappa_y=-0.1$. The ω/ω_0=constant curves change direction. It may be seen that now both waves in zone V are backward waves. The frequency ranges of the nine zones are given by Eq. (15). All the curves traverse several zones, starting in zone III and ending in zone VII.

Next we choose a case when there is negative coupling in the x direction ($\kappa_x=-0.05$) and much larger positive coupling in the y direction ($\kappa_y=0.3$). The wave is now backward in the x direction and forward in the y direction as may be seen in Fig. 5(b). The major consequence of high coupling in the y direction is that the main pass band is wide in the y direction and narrow in the x direction.

In the traditional representation the ω/ω_0=constant curves are confined to zone V. In our generalized representation any of the constant ω/ω_0 curves traverse several zones showing that at a given frequency a number of different kinds of wave behavior are possible. There is however a conceptual difficulty. When considering a dispersion equation we always think of infinite plane waves propagating in an infinite lattice in the x and y directions. This traditional picture can no longer be applicable when evanescent waves are also included in the picture. It is possible of course to

imagine that (say) in zone II the wave propagates in the x direction and decays monotonically in the y direction, however the association with infinite dimensions appears to be less justified. One could legitimately ask, where does the wave decay away from? From infinity? It does not make much sense. Hence to envisage what is going on we should resort to finite structures. As an example we shall take 29 $\times$29 resonant ring elements in a rectangular lattice. We shall explore the possibilities of excitation of evanescent modes in Sec. VI after a brief discussion of spatial resonances which are always relevant when propagating waves in a finite lattice are involved.

We need to note here that our representation, giving the full information contained in the dispersion equation, is made possible by neglecting Ohmic losses. We can do so because the fundamental physical difference is between propagating and evanescent waves. Ohmic losses are significant only in those cases when information has to be carried by a guided wave for a long distance, e.g., across the Atlantic.

V. EIGENFUNCTIONS AND SPATIAL RESONANCES

The ω/ω_0=constant curves being continuous suggests that all points in the dispersion diagram are achievable. This is true for an infinite lattice. For a finite lattice only certain variations are permissible determined by the eigenfunctions. For a linear lattice containing N elements the current eigenfunctions are given simply[15] as

$$I_l(n) = A_l \sin\left(\frac{\pi l n}{N+1}\right), \tag{17}$$

where A_l is a constant, l is the order of the eigenfunction and n is the running variable from element to element. For a 2D rectangular $N_x \times N_y$ lattice the same functions appear in both directions,

$$I_{l_x,l_y}(n_x,n_y) = A_{l_x,l_y} \sin\left(\frac{\pi l_x n_x}{N_x+1}\right)\sin\left(\frac{\pi l_y n_y}{N_y+1}\right). \tag{18}$$

We may call it a spatial resonance when the current distribution is given by its eigenfunction. A finite lattice being a discrete structure, the currents do not vanish at the edges, as it would be for a continuous structure. Instead the currents are taken zero in the fictional elements located next to the edges.

VI. EVANESCENT MODE EXCITATION

We shall now take a 29$\times$29 rectangular lattice with κ_x=−0.1 and κ_y=0.1 and excite waves, propagating or evanescent, in each one of the new zones. Let us first choose zone VIII. Any point within this zone denotes a wave that propagates in the x direction as $\exp(i\zeta_x' n_x)$ and decays in the y direction as $(-1)^{n_y}\exp(-\zeta_y'' n_y)$. At least this is the prediction of the dispersion Eq. (6) valid, as mentioned, for an infinite lattice. Is it valid for a finite lattice as well? To check that we shall choose point P_1 in zone VIII on the ω/ω_0=0.9 curve with $\zeta_x=\pi/10$ and $\zeta_y=\pi+i0.274\pi$ as shown in Fig. 4. The

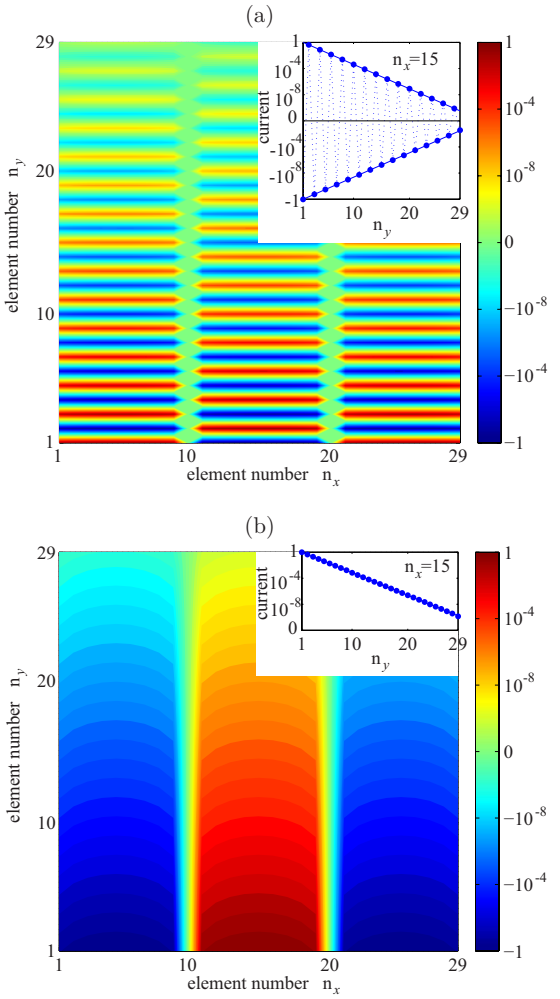

FIG. 6. (Color online) 2D current distribution for P_1 in zone VIII (a) and P_2 in zone II (b). Insets show the variation of the current along the central vertical line of the 2D structure. Dots: the generalized Kirchhoff equation; solid line: dispersion equation.

value of ζ_x' is of particular importance. For an effective excitation the imposed variation must coincide with one of the eigenfunctions. We shall impose a voltage variation upon the first line of the 29$\times$29 lattice as given by

$$V(n_x) = V_0 \sin\left(\frac{3\pi n_x}{30}\right), \tag{19}$$

which is one of the eigenfunctions. The resulting current distribution, simulated by GKE, a magnetoinductive surface wave, is shown in Fig. 6(a). The code (logarithmic in amplitude but showing both positive and negative values) is chosen so that dark red and dark blue denote high positive and high negative values, respectively (note that the continuous variation of the color carries no information, it is valid only in the discrete points defined by the position of the elements). As expected the variation in the x direction corresponds to the imposed pattern and there is alternating decline in the y direction. For a more accurate quantitative comparison of the decay we can choose line n_x=15, where the current is maximum, and plot the current for all the elements in

that line. This is shown in the inset to Fig. 6(a) using again a scale logarithmic in amplitude but showing both positive and negative values. The linear decay scale shows that the function is indeed exponential, while the sign is changing from element to element along the y direction. The rate of decay obtained by GKE is shown by dots whereas that coming from the dispersion equation by solid lines. The agreement may be seen to be excellent. This is our first proof that the dispersion equation usually associated with infinite dimensions is meaningful, and predicts the correct variation for exponential decay for a finite lattice as well. Remaining in the same zone, for any frequency in the corresponding range given by Eq. (14) we can choose any point with coordinates $\zeta_x = \pi l/30 (l=1,\ldots,29)$ and ζ_y provided by dispersion Eq. (6). The conclusions remain unchanged: the response of the metamaterial structure obtained by GKE shows a surface wave propagating in the x direction with the imposed wave number in the x direction and with the rate of current decay in the y direction being very accurately predicted by the dispersion equation.

Our next example, point P_2 in zone II, lies on the $\omega/\omega_0 = 1.02$ curve, and the excitation pattern is the same as for point P_1. P_2 has coordinates $\zeta_x = \pi/10$ and $\zeta_y = i0.255\pi$. The current distribution is shown in Fig. 6(b). The surface wave still propagates in the x direction, but the decline in the y direction is now monotonic and slower than that in P_1. A quantitative comparison of the decay along the line $n_x = 15$ predicted from the dispersion equation and obtained by GKE is shown in the inset and may be seen to be excellent. There is an essential difference between point P_2 and point P_1 from the previous example. The $\omega/\omega_0 = 1.02$ curve may be seen to traverse zone V, thus allowing for solutions propagating in both directions. However, as no propagating eigenmodes of Eq. (18) are excited at the chosen frequency, the required surface-wave solution is successfully imposed.

We can draw very similar conclusions by taking points in any of the zones II, IV, VI, and VIII: if a wave propagates in one direction and decays in the other direction then the predictions of the dispersion equation apply also to finite structures.

However, zones I, III, VII, and IX are in a different category. The waves decline in both directions. It is intuitively obvious that imposing that decay in one direction along one boundary is insufficient to ensure a decay in the other direction predicted by the dispersion equation. Our intuition suggests that, for any of the new zones, excitation by imposing a voltage decaying along a single boundary would not work. Our simulations confirm it. There is however hope that we can reproduce the required current distribution by imposing a voltage distribution upon the first lines both in the x and y directions. This is what we do when we choose point P_3 with coordinates $\zeta_x = i0.408\pi$ and $\zeta_y = \pi + i0.4\pi$ on the $\omega/\omega_0 = 0.85$ curve in zone VII. The corresponding current distribution is shown in Fig. 7(a). The decay in both directions (monotonic in the x and alternate in the y direction) can be clearly seen. To check whether we were successful imposing the decay in both direction upon the whole lattice, we plot the decay in the x and y directions in Figs. 7(b) and 7(c) for a number of lines x=constant and y=constant within the structure. The decay curves (plotted on the logarithmic scale)

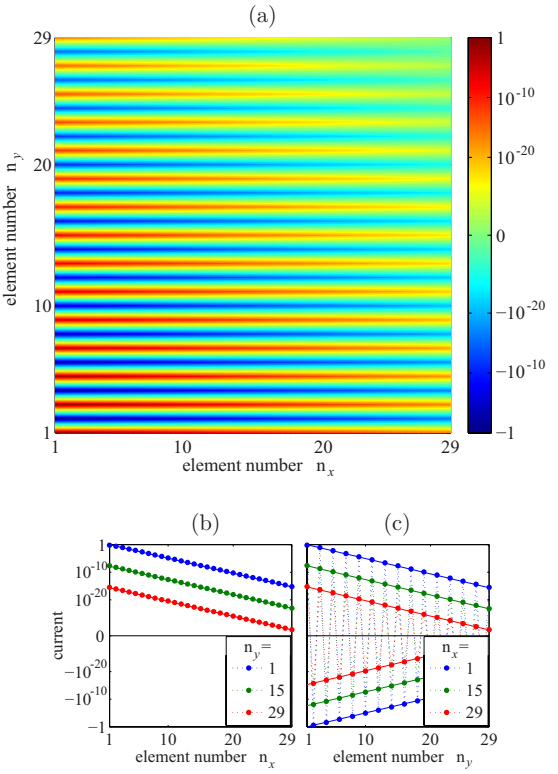

FIG. 7. (Color online) (a) 2D current distribution for P_3 in zone VII. The variation in the current along selected (b) horizontal and (c) vertical lines of the 2D structure. Dots: the generalized Kirchhoff equation; solid line: dispersion equation.

being parallel lines is a proof that we did indeed succeed to impose the decay upon the whole lattice. Also in this case, the dots representing the values of the currents retrieved by the GKE method lie on the solid lines of the solutions predicted by the dispersion equation. Following the same procedure, we can choose any point in zone VII or III, impose the decays upon both boundaries and find that the resulting current distribution agrees with that predicted by the dispersion equation.

For a planar-axial configuration, there is a major difference between zones III and VII, on one side, and zones I and IX, on the other side. Solutions from zones III and VII, decaying in both directions, can successfully be imposed by excitation decaying along two boundaries of a 2D finite structure, whereas solutions from zones I and IX cannot. Why? Point P_3, and, generally, any point in zone VII, lies on an isofrequency which traverses zone IV with a larger attenuation in the x direction than that of P_3, and zone VIII with a larger attenuation in the y direction than that of P_3. The solution P_3, having the smallest decay, can successfully be imposed. The same applies to zone III—a solution is imposed because it has a small decay in comparison with competitors from zones II and VI. The situation is reversed if we choose, say, point P_4 in zone I, remaining on the same isofrequency. Excitation with a decay in the x direction determined by P_4 will not be reproduced in the current distribution because lower decays on the same isofrequency curve are available in zone IV propagating in the y direction. The same is true if we choose a point in zone I on an isofre-

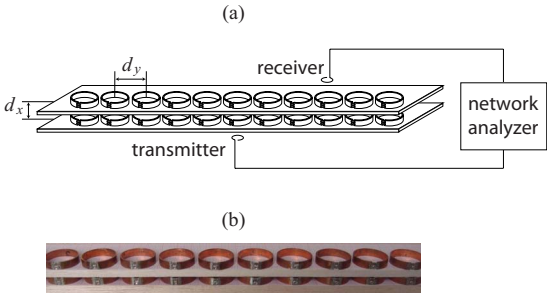

FIG. 8. (Color online) Magnetoinductive lens. (a) Schematic representation and (b) photograph of the experimental setup.

quency curve traversing zone II. Hence, again, the distribution predicted by the infinite lattice model will not be reproduced. Whatever has been said about zone I will also apply to zone IX. Lower attenuation will be available in zone VI or VIII. Similar conclusions can be drawn for the planar-planar configuration but in that case the zones in which the method of excitation fails to reproduce the current distributions predicted by the dispersion equation are zones III and VII.

We have to emphasize here that the failure to reproduce current distributions in certain zones does not affect the usefulness of the representation. The generalized Brillouin diagram with its nine zones offers an instant recognition of the important properties of the waves in the stop bands, that how large is the attenuation at different frequencies, which are the solutions which propagate in one direction and decay in the other direction, and what are the likely consequences of certain excitations. The zones in which there is decay in both directions have limited significance. The only practical case we can think of is an evanescent surface wave with moderate attenuation.

VII. MECHANISM OF THE MAGNETOINDUCTIVE LENS

So far all our examples have been concerned with 29×29 lattices. We shall add here a rather extreme example in the sense that it has only two elements in the x direction barely qualifying as a 2D structure. We shall take 2 strongly coupled elements in the axial configuration in the x direction, and 15 weakly coupled ones in the planar configuration in the y direction. This configuration, shown schematically in Fig. 8(a), is a variety of the so-called magnetoinductive lens[30] and it has already been interpreted as a one-dimensional biatomic metamaterial chain[31,32] which allows for subwavelength imaging precisely at the resonant frequency of individual ring resonators. In the nearest-neighbor approximation for two identical lines the dispersion equation was found in the form

$$1 - \frac{\omega_0^2}{\omega^2} + \kappa_y \cos \zeta_y = \pm \frac{\kappa_x}{2}. \tag{20}$$

The two solutions in Eq. (20) mean that, given the suitable combination of the coupling coefficients κ_x and κ_y, the pass band is split into two with a stop band in between. The essential criterion is that sideways propagation of MI waves must be prohibited.

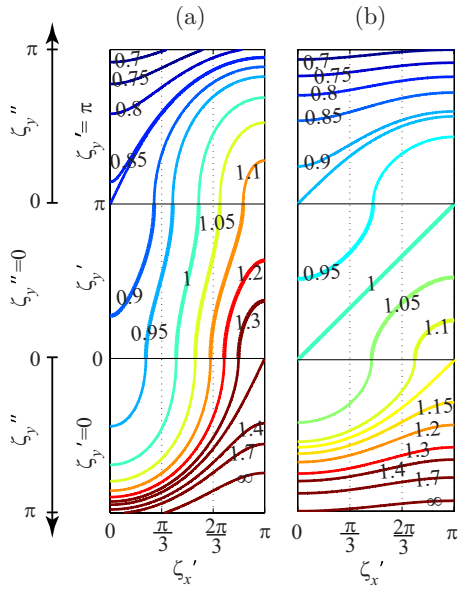

FIG. 9. (Color online) Magnetoinductive lens with strong coupling in the y direction, $\kappa_x=0.45$ and $\kappa_y=-0.1$ (a) and with weak coupling, $\kappa_x=0.1$ and $\kappa_y=-0.1$ (b). Only zones II, V, and VIII are shown.

We shall now analyze the properties of the magnetoinductive lens with the aid of our extended 2D Brillouin diagram. The $\omega/\omega_0=$constant curves for this case are plotted in Fig. 9(a), using the measured values (for a brief description of the measurements see below) of the coupling coefficients, $\kappa_x=0.45$, $\kappa_y=-0.1$. It needs to be noted, only zones II, V, and VIII are shown. Having only two elements in the x direction the two eigenfunctions are

$$I(n_x) = \sin\left(\frac{\pi n_x}{3}\right) \quad \text{and} \quad I(n_x) = \sin\left(\frac{2\pi n_x}{3}\right), \tag{21}$$

the two lines being in phase for the first one and in antiphase for the second one. In the x direction the only allowed solutions are $\zeta_x'=\pi/3$ and $2\pi/3$ denoted by dashed lines in Fig. 9(a). This means that for any $\omega/\omega_0=$constant curve the value of ζ_y' in zone V or the values of ζ_y'' in zones II and VIII are given by the intersection of those curves with the dashed lines.

Let us first choose $\zeta_x'=\pi/3$. We can see from Fig. 9(a) that the intersections are below $\omega/\omega_0=0.87$ in zone VIII and above $\omega/\omega_0=0.95$ in zone II, and there is one pass band between the two stop bands. This is shown by the continuous blue curve on the left-hand side of Fig. 10 where ζ_y'' is plotted as a function of frequency. Note that in the pass band $\zeta_y''=0$. We can repeat the exercise by choosing $\zeta_x'=2\pi/3$. Then the stop bands are below $\omega/\omega_0=1.07$ and above $\omega/\omega_0=1.22$. The intersections of the $\omega/\omega_0=$constant curves in zones II and VIII will give again the rate of decay in the y direction. These results are plotted on the right-hand side of Fig. 10(a) by the continuous red line. There is again a pass band between the two stop bands, similarly to that on the left-hand side. The interesting, and rather unexpected, thing is that there is now a stop band in the middle of the pass band of the

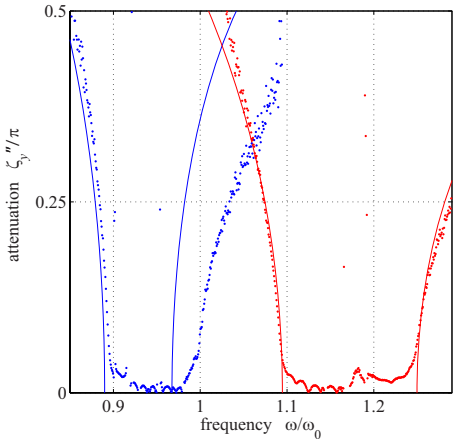

FIG. 10. (Color online) Magnetoinductive lens. Decay rate versus frequency as predicted by the dispersion equation (thin solid line) as well as retrieved from the experimental data (dots).

single line. There is no propagation at the resonant frequency of the elements. We can use again the GKE simulation to see whether specifying the frequency and ζ_x' for this 2×15 lattice will yield the values of ζ_y'' predicted by the dispersion equation. From the experience obtained by simulations in Section VI we can be fairly certain that exercise will succeed, and indeed the attenuation curves obtained by simulations coincide quite closely with those (both on the left-hand side and on the right-hand side) plotted in Fig. 10. There is no need to show them.

We have also performed experiments to confirm the theoretical results in this particular case of two coupled lines. It consisted of 2×15 elements as shown schematically in Fig. 8(a) and on the photograph of Fig. 8(b). The measurement setup was identical with that reported in Refs. 31 and 32. The elements consisted of singly split loops (mean radius of 11 mm) loaded by capacitors with a resonant frequency of 51.7 MHz and a quality factor of 165. The coupling coefficients were measured separately; their values have already been given above for calculating the theoretical curves. The array was excited either in the middle or at one of the edges by a small transmitter coil and the current was measured by a similar receiving coil. The attenuation, calculated from the measured currents, is shown in Fig. 10 by dots. The agreement with the theoretical results is quite reasonable.

Whether the magnetoinductive lens is suitable for subwavelength imaging at the resonance frequency depends critically on the values of the coupling coefficients. Figure 9(b) shows the ω/ω_0=constant curves for the case when the separation between the coupled lines is very much reduced so that κ_x declines to 0.1. It is still true of course that the pass bands are different for the $\zeta_x'=\pi/3$ and $2\pi/3$ excitations but now the two pass bands overlap and the magnetoinductive lens is not working at ω_0.

It is worth mentioning a very simple rule for deciding whether the two pass bands overlap. We need to look at the ω/ω_0=constant curves and see whether there are any which can traverse zone V without touching either of the dashed lines. In Fig. 9(a) the $\omega/\omega_0=1$ curve clearly has this property. In the counterexample of Fig. 9(b), where the coupling is reduced, no such curve exists. Thus, for the 2D magnetoinductive lens made of two chains of resonant elements to work at the resonant frequency ω_0, the condition

$$|\kappa_y| > 2|\kappa_x| \tag{22}$$

has to be fulfilled. Our conclusion is that the imaging mechanism of the magnetoinductive lens is quite different from the mechanism of Pendry's superlens. In the superlens, a requirement is that two slow-wave modes (e.g., surface-plasmon polaritons) propagating along two closely spaced surfaces couple to each other enabling the transfer of the near-field information across the structure. In the case of the magnetoinductive lens, however, waves do not propagate but decay along each of the two surfaces, and propagate across the structure in the direction perpendicular to both surfaces.

VIII. CONCLUSIONS

Propagating and evanescent waves for two-dimensional periodic structures have been studied. By adding eight new zones to the traditional first Brillouin zone we have been able to include in graphical form the full information contained in a lossless dispersion equation. The generalization has been tested by considering MI waves in a two-dimensional lattice of capacitively loaded loops. The applicability of the dispersion curves to finite lattices has been investigated by the generalized Kirchhoff equations (GKE). The examples involve 29×29 element lattices in the planar-axial and in the planar-planar configurations. The mechanism of the magnetoinductive lens is unraveled and shown to be quite different from Pendry's superlens as it involves not coupled surfaces but evanescent waves decaying along the surfaces and propagating into the depth of the structure. We wish to emphasize that MI waves employed here are not the only candidates for showing the relationships between evanescent and propagating waves. Our method is directly applicable to all periodic systems capable of supporting slow waves by virtue of coupling between the elements. In particular, generalized Brillouin diagrams can be used to describe waves of coupling between nanoparticles and employed for the design of near-field manipulating devices. This approach can easily be adjusted to other types of coupling including electric coupling[23,28] and coupling in connected ring chains.[21] The approach being valid for any resonant frequency will be useful in the design and analysis of nanostructured metamaterials for THz and visible frequencies by accounting for both propagating and evanescent slow-wave modes. Finally, we wish to note that our representation need not be restricted to periodic structures. Nonperiodic media may also have dispersion equations with both propagating and evanescent waves in the solution although in that case radiation problems are more likely to cause complications for finite structures.

ACKNOWLEDGMENT

E.T. and E.S. gratefully acknowledge funding by the German Research Foundation (SAOT and Emmy Noether Programme).

*Corresponding author; ekaterina.shamonina@aot.uni-erlangen.de

[1] G. Lippmann, J. Phys. (Paris) **3**, 97 (1894).
[2] W. Friedrich, P. Knipping, and M. von Laue, Sitzungsberichte der (Kgl.) Akad. der Wiss. Bayer, 303 (1912).
[3] L. Brillouin, *Wave Propagation in Periodic Structures* (Dover, New York, 1953).
[4] R. Peierls, Ann. Phys. **12**, 154 (1932).
[5] J. D. Joannopoulos, S. G. Johnson, J. N. Winn, and R. D. Meade, *Photonic Crystals: Molding the Flow of Light*, 2nd ed. (Princeton, Princeton, NJ, 2008).
[6] Y. C. Hsue and T. J. Yang, Phys. Rev. E **70**, 016706 (2004).
[7] Y. C. Hsue, A. J. Freeman, and B.-Y. Gu, Phys. Rev. B **72**, 195118 (2005).
[8] P. Baccarelli, S. Paulotto, D. R. Jackson, and A. A. Oliner, IEEE Trans. Microwave Theory Tech. **55**, 1484 (2007).
[9] J. B. Pendry, Phys. Rev. Lett. **85**, 3966 (2000).
[10] C. Rockstuhl, C. Menzel, T. Paul, T. Pertsch, and F. Lederer, Phys. Rev. B **78**, 155102 (2008).
[11] C. Tserkezis, N. Papanikolaou, G. Gantzounis, and N. Stefanou, Phys. Rev. B **78**, 165114 (2008).
[12] X. Zhang, M. Davanco, Y. Urzhumov, G. Shvets, and S. R. Forrest, Phys. Rev. Lett. **101**, 267401 (2008).
[13] A. V. Kats, S. Savelev, V. A. Yampolskii, and F. Nori, Phys. Rev. Lett. **98**, 073901 (2007).
[14] E. Shamonina, V. A. Kalinin, K. H. Ringhofer, and L. Solymar, Electron. Lett. **38**, 371 (2002).
[15] E. Shamonina, V. A. Kalinin, K. H. Ringhofer, and L. Solymar, J. Appl. Phys. **92**, 6252 (2002).
[16] M. C. K. Wiltshire, E. Shamonina, I. R. Young, and L. Solymar, Electron. Lett. **39**, 215 (2003).
[17] M. C. K. Wiltshire, E. Shamonina, I. R. Young, and L. Solymar, J. Appl. Phys. **95**, 4488 (2004).
[18] A. Radkovskaya, M. Shamonin, C. J. Stevens, G. Faulkner, D. J. Edwards, E. Shamonina, and L. Solymar, J. Magn. Magn. Mater. **300**, 29 (2006).
[19] G. Dolling, M. Wegener, A. Schädle, S. Burger, and S. Linden, Appl. Phys. Lett. **89**, 231118 (2006).
[20] H. Liu, D. A. Genov, D. M. Wu, Y. M. Liu, J. M. Steele, C. Sun, S. N. Zhu, and X. Zhang, Phys. Rev. Lett. **97**, 243902 (2006).
[21] T. Li, R. X. Ye, C. Li, H. Liu, S. M. Wang, J. X. Cao, S. N. Zhu, and X. Zhang, Opt. Express **17**, 11486 (2009).
[22] A. Alu and N. Engheta, Opt. Express **17**, 5723 (2009).
[23] N. Liu, S. Kaiser, and H. Giessen, Adv. Mater. **20**, 4521 (2008).
[24] E. Shamonina, Phys. Status Solidi B **245**, 1471 (2008).
[25] L. Solymar and E. Shamonina, *Waves in Metamaterials* (Oxford University Press, Oxford, 2009).
[26] R. R. A. Syms, E. Shamonina, V. Kalinin, and L. Solymar, J. Appl. Phys. **97**, 064909 (2005).
[27] J. D. Baena, L. Jelinek, R. Marques, and M. Silveirinha, Phys. Rev. A **78**, 013842 (2008).
[28] M. Beruete, F. Falcone, M. J. Freire, R. Marques, and J. D. Baena, Appl. Phys. Lett. **88**, 083503 (2006).
[29] W. H. Weber and G. W. Ford, Phys. Rev. B **70**, 125429 (2004).
[30] M. J. Freire and R. Marques, Appl. Phys. Lett. **86**, 182505 (2005).
[31] O. Sydoruk, M. Shamonin, A. Radkovskaya, O. Zhuromskyy, E. Shamonina, R. Trautner, C. J. Stevens, G. Faulkner, D. J. Edwards, and L. Solymar, J. Appl. Phys. **101**, 073903 (2007).
[32] O. Sydoruk, A. Radkovskaya, O. Zhuromskyy, E. Shamonina, M. Shamonin, C. J. Stevens, G. Faulkner, D. J. Edwards, and L. Solymar, Phys. Rev. B **73**, 224406 (2006).
[33] O. Sydoruk, E. Shamonina, and L. Solymar, Microwave Opt. Technol. Lett. **49**, 2228 (2007).